Available online at www.sciencedirect.com
SCIENCE DIRECT
ELSEVIER
Journal of Physics and Chemistry of Solids 66 (2005) 1609–1613
JOURNAL OF PHYSICS AND CHEMISTRY OF SOLIDS
www.elsevier.com/locate/jpcs

The structure and optical properties of AlN nanocrystals prepared by Schlenk techniques at atmospheric pressure and low temperature

S.X. Lu[a,b], Y.H. Tong[c], Y.C. Liu[a,*], C.S. Xu[a], Y.M. Lu[c], J.Y. Zhang[c], D.Z. Shen[c], X.W. Fan[c]

[a]*Center for Advanced Optoelectronic Functional Material Research, Northeast Normal University, Changchun 130024, P.R. China*
[b]*College of Chemistry, Jilin University, Changchun 130021, P.R. China*
[c]*Key Laboratory of Excited State Processes, Changchun Institute of Optics, Fine Mechanics and Physics, Chinese Academy of Sciences, Changchun Economic Exploitation Region, 16-East South-lake Avenue, Changchun 130033, P.R. China*

Received 26 August 2004; revised 1 February 2005; accepted 8 June 2005

Abstract

AlN nanocrystals were prepared in organic solvent at atmospheric pressure and low temperature by the Schlenk technique. Both hexagonal and cubic AlN nanocrystals were obtained. The hexagonal nano-AlN powder possessed a wurtzite structure with $a=3.124$ Å, $c=5.024$ Å, the average grain size was about 2 nm. The lattice constant of the cubic nano-AlN was $a=9.171$ Å, the average grain size was about 4 nm. The structural and optical properties of the obtained AlN were analyzed. The emission related to deep-level defects was investigated by using temperature-dependent photoluminescence.

Keywords: A. Nanostructures; B. Chemical synthesis; D. Photoluminescence

1. Introduction

Wide-band-gap-semiconductor Aluminum Nitride (AlN) has numerous properties (such as high temperature stability, high thermal conductivity and high elasticity [1–4]), which make it attractive for potential applications in laser diodes, solar blind Photodiodes (PD), blue/UV Light Emitting Diodes (LED) and high-temperature/high-power electronic devices [5–6]. Recently, there have been considerable interests in the luminescence properties of AlN nanocrystals [6–9], which can demonstrate enhanced luminescence intensity due to the quantum size effect. Quantum confinement can also reveal other unique properties that are not observed in the bulk material. Although the conventional direct nitridation synthesis is an effective method for the large-scale production of commercial AlN powders, it requires high temperature or high-pressure condition. Consequently, applications of AlN may be limited because of the high price of the raw material. Therefore it is necessary to find better methods to obtain AlN nanocrystals. This paper reported the results of investigations of the structural and optical properties of AlN nanocrystals synthesized at atmospheric pressure and low temperature by Schlenk techniques. The origin of luminescence was analyzed with the help of temperature-dependent Photoluminescence (PL) spectra from 81 to 294 K.

2. Experimental details

The reaction was carried out in a high-purity Ar atmosphere by using Schlenk techniques [10]. Prior to use, xylene was refluxed over sodium strips with benzophenoneketyl until it turned blue and then distilled. Anhydrous $AlCl_3$ and Li_3N were purchased from Aldrich and used without further purification.

Samples I and II: Li_3N (0.2292 g, 6.6 mmol) and Li_3N (0.1409 g, 4.0 mmol) were added to the solutions of $AlCl_3$ (0.8240 g, 6.2 mmol) and $AlCl_3$ (0.5926 g, 4.5 mmol) in 100 mL of xylene, respectively, stirred simultaneously for 24 h at 110 °C in an Ar ambient condition. The mixtures were then poured to 100 mL ice water in which several

* Corresponding author. Tel.: +86 431 509 8803; fax: +86 431 568 4009.
E-mail address: ycliu@nenu.edu.cn (Y.C. Liu).

0022-3697/$ - see front matter © 2005 Elsevier Ltd. All rights reserved.
doi:10.1016/j.jpcs.2005.06.007

pieces of quartz film prepared for measuring UV absorption spectra, respectively, stirred vigorously until the color of precipitate turned into milk white, and then filtered and rinsed with water on a G_4 glass–sand filter. The products were dried in a vacuum oven at 80 °C for 2–3 h, yielding samples I and II.

The reaction could be expressed as Scheme 1.

$$AlCl_3 + Li_3N \rightarrow AlN + 3LiCl$$

Scheme 1.

Infrared spectra were measured using a Nicolet FTIR 760 infrared spectrometer. X-ray Diffraction (XRD) patterns were collected on a Rigaku D max-γA X-ray diffractometer, with Ni filtered Cu K_α radiation of 1.54 Å (50 kV, 100 mA) and scanning speed of 4°/min. PL were excited by the 325 nm line of a He–Cd laser (50 mW). The laser beam was focused to a spot of 30 μm in diameter. The monochromator used for the PL measurements had a grating of 600 groove/mm with a blaze wavelength of 500 nm. Luminescence signals were recorded using a Jobin Yvon ultraviolet microlaser Raman spectrometer. UV absorption spectra were measured with a Cary 50 Violet-visible spectrometer.

The as-synthesized sample I was divided into several parts, four of them were annealed for 1 h in N_2 atmosphere at temperatures of 100, 200, 400 and 600 °C, respectively, corresponding to samples A1, A2, A3 and A4 (Here, the as-synthesized part was designated as A0). Sample II was divided into several parts and three of them were annealed for 1 h in Ar atmosphere at temperatures of 200, 400 and 600 °C, respectively, corresponding to samples B1, B2 and B3 (Here, the as-synthesized part of sample II was designated as B0).

3. Results and discussion

Fig. 1 shows the XRD patterns for some of the samples. For sample I, the peaks at $2\theta = 33.11$, 36.03, 38.43 and 47.50° can be attributed to the wurtzite structure with lattice parameters $a = 3.124$ Å and $c = 5.024$ Å. The parameters are in good agreement with the previously reported values ($a = 3.112$ Å, $c = 4.982$ Å) of AlN single crystals [11]. The calculated density of the powder is 3.2 g/cm^3 at room temperature, which is similar to that of the AlN single crystals (3.257 g/cm^3) grown by sublimation [11]. For sample II, the transition from wurtzite to cubic phase can be verified by XRD results. For sample B0 without annealing, the peaks at $2\theta = 33.23$, 36.29, and 38.31° come from the wurtzite structure, while the peak at $2\theta = 38.79°$ comes from the cubic structure; the diffraction patterns vary with the increase of annealing temperature, for the sample B1 annealed at 200 °C, the diffraction peak from wurtzite AlN at $2\theta = 33.23$ disappears, at the same time,

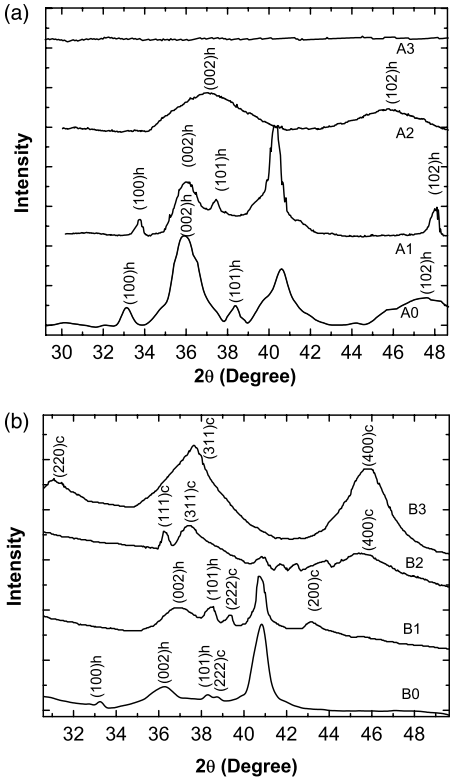

Fig. 1. XRD spectra of AlN nanoparticles: (a) sample I and (b) sample II.

the characteristic diffraction peak from cubic AlN at $2\theta = 43.50$ emerges. When the annealing temperature is raised to 400 °C (sample B2), the intensities of the characteristic peaks of cubic AlN at $2\theta = 36.24$, 37.51, and 45.63° increase. When the annealing temperature is further raised to 600 °C (sample B3), the XRD diffraction pattern completely changes into that of cubic structure, as shown in Fig. 1(b). The lattice constant of the crystallites in sample B3 is $a = 9.171$ Å.

The average particle size can be estimated from the Scherrer Eq.

$$D_{hkl} = k\lambda/\beta_{hkl} \cos \theta_{hkl}$$

where D_{hkl} is the average particle size, k is a constant, β_{hkl} and θ_{hkl} are the full width at half maximum and the Bragg angle of the (hkl) diffraction peak, respectively, and λ is the X-ray wavelength.

The average particle size of the obtained AlN of sample I increases with the increase of annealing temperature from 80 to 150 °C. At 80 °C (A0) the size is 4 nm, at 100 °C (A1) the size is 5 nm, and at 150 °C the size is 7 nm. However, the size decreases to 2 nm for the 200 °C (A2) annealing temperature case. At 400 °C (A3) and 600 °C (A4), all the peaks in the XRD spectra disappear (Fig. 1a, A4 is the same as A3); indicating that AlN was became amorphous phase for the annealing temperature higher than 400 °C. For the sample II: at 80 °C (B0) the size is 6 nm, at 200 °C the size is 5 nm, at 600 °C the size is 4 nm. The structure of sample II transfers from hexagonal AlN phase to cubic AlN phase

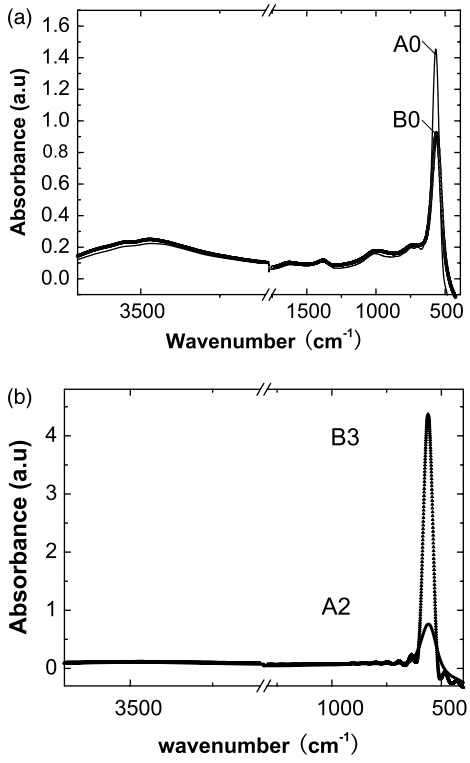

Fig. 2. FTIR absorption spectra of AlN nanoparticles of samples I and II. (a) As-synthesized AlN; (b) A2: wurtzite AlN nanocrystals, B3: Cubic AlN nanocrystals.

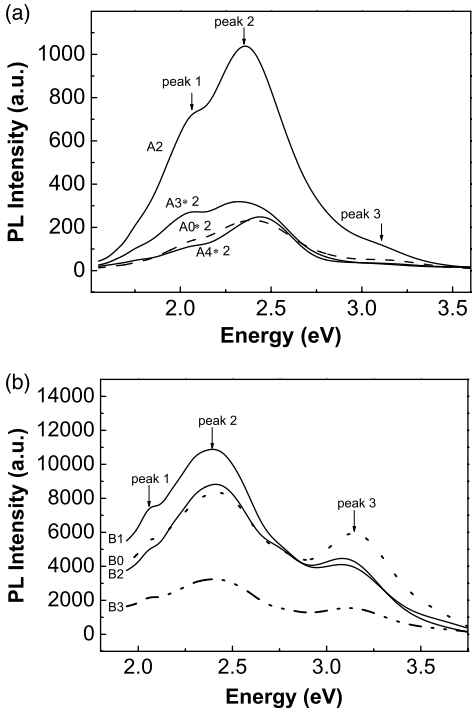

Fig. 3. Room temperature PL spectrum excited at 325 nm for AlN nanoparticles (a) for sample I (b) for sample II.

when the annealing temperature is higher than 150 °C. The peak at $2\theta = 40.51°$ in Fig. 1a and b corresponds to the impurity $Al(OH)_3 \cdot LiCl \cdot nH_2O$ on the surface of AlN nanocrystals. This can be confirmed by FTIR (see Fig. 2), X-ray and Photoluminescence spectra. From FTIR, the peak at 3472 cm^{-1} can be attributed to O–H vibration of water and $Al(OH)_3$ absorbed on the nanocrystal surface. The peak of $2\theta = 40.51°$ disappears when AlN is annealed at 200 °C, the peak positions of photoluminescence spectra (see Fig. 3) do not change. Hao et al., [8] had demonstrated that hexagonal AlN phase and cubic AlN phase co-exist by TEM when the reactant proportion of $AlCl_3$ and Li_3N is 1:1. The main reason why the structure of sample II transfers from hexagonal AlN phase to cubic AlN phase may be that the excessive $AlCl_3$ leads conversion of crystal lattice. The reactant proportion of $AlCl_3$ and Li_3N determines the structure of crystal lattice.

In order to determine the optical band gap of the AlN film, both transmittance T and reflectance R are converted to absorbance α, in terms of $\alpha = (1/d)\ln((1-R)/T)$, and $\alpha + R + T = 1$. The direct optical gap E_g is determined by extrapolating the function

$$(\alpha E)^2 = B(E - E_g)$$

to the horizontal axis (energy), where B is a proportionality constant which reflects the integrality of the crystal lattice. Fig. 4 shows the graph of $(\alpha E)^2$ versus E for the film grown on quartz. The film is annealed at 200 °C (A2), 400 °C (A3) and 600 °C (A4). In Fig. 4, all samples exhibit broad absorption from 6.52 to 1.55 eV. A sharp absorption is found to be near 6.52 eV. As shown in the inset of Fig. 4, the band gap energy E_g is 6.18 eV for A0, 6.39 eV for A2, 6.31 eV for A3 and 6.29 eV for A4.

FTIR spectra, as shown in Fig. 2, were measured to determine the composition and structure of AlN powder. Fig. 2(a) shows the following IR (KBr) peaks (in cm^{-1}) for A0 and B0: 3472, 1623, 1362, 1005, 735 and 562. The peak of 562 cm^{-1}, which corresponds to AlN, is stronger for A0 than that for B0, while the other peaks for sample A0 are

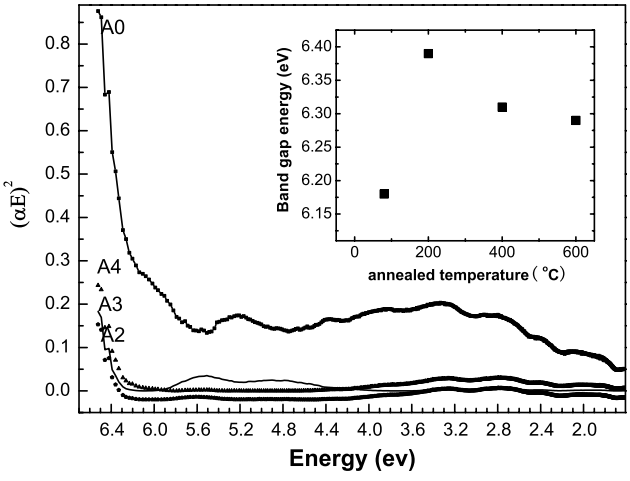

Fig. 4. UV absorption edge of AlN nanoparticles of sample I.

weaker than that for B0. The reason why the peak of 562 cm^{-1} for A0 is stronger than that for B0 is that the quantity of AlN nanoparticles in A0 is more than that in B0. Fig. 2(b) shows only the peak at 562 cm^{-1} for samples A2 and B3. For sample B3, the peak is stronger than that of sample A2. The reason why the peak at 562 cm^{-1} of B3 is stronger than that of A2 is that the lattice structure of the AlN particles in B3 is different from that in A2. The peaks at 3472, 1623, 1362, 1005 and 735 cm^{-1} are from impurity. The peaks at 3472 and 1623 cm^{-1} are vibrational modes of O–H, the peak at 1362 cm^{-1} is swing vibrational mode of O–H. The peaks at 1005 and 735 cm^{-1} are swing vibrational modes of O–H of $Al(OH)_3$. Hao et al. [8] has recognized the 1005 cm^{-1} peak as the TO phonon of cubic AlN, but in our work, the peak at 1005 cm^{-1} appeared in Sample I without cubic AlN. Because the peaks to be larger than 600 cm^{-1} disappear with increased annealing temperature, those peaks can be attributed to OH vibrational modes.

Fig. 5 shows the room-temperature Raman spectra of as-synthesized AlN recorded using the 325 nm line of a He–Cd laser. The peak positions are 587, 1040, 1361 and 1610 cm^{-1} for A0, 587, 1361 and 1610 cm^{-1} for B0 and B3. The phonon frequency of AlN nanoparticles is 587 cm^{-1}. Compared with the frequency (602, 654 cm^{-1}) of the AlN nanoparticles with a diameter of about 32 nm [5], the low-wave-number shift of phonon frequency is the result of the nanosize effect. The peaks of sample II are stronger than that of sample I. There is no 1040 cm^{-1} peak in sample II. The peaks at 1040, 1361 and 1610 cm^{-1} are from impurities, as supported by examination of the FTIR spectra.

Fig. 3 shows room-temperature photoluminescence spectra of the AlN samples excited at 325 nm. There is a wide emission band ranging from 1.55 to 3.76 eV. Sample A2 gives the strongest integrated intensity of the wide emission band (see Fig. 3(a)). This can be explained in terms of the XRD results. From XRD results the average particle size of the as-synthesized AlN is estimated at 4 nm, and the average size of the AlN powder annealed at 200 °C (sample A2) is estimated at 2 nm. The AlN powder becomes amorphous for the annealing temperature higher than

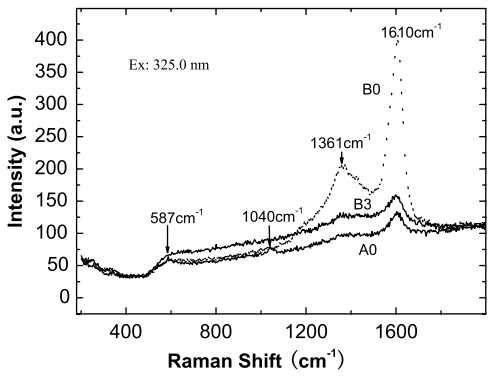

Fig. 5. Raman scattering spectra of AlN nanoparticles.

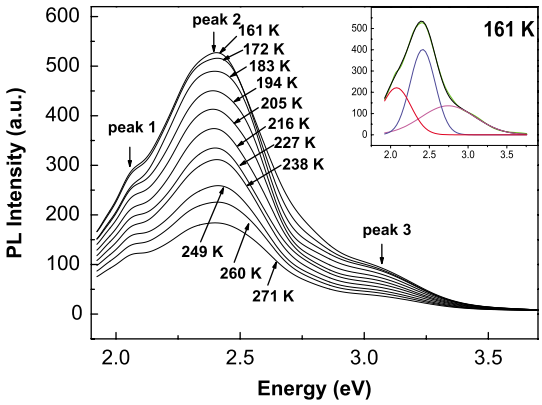

Fig. 6. Temperature-dependent PL spectrum excited at 325 nm for as-synthesized AlN nanoparticles A0.

200 °C. The AlN annealed at 200 °C takes on special character because of its small size (2 nm) due to degradation of the nanocrystals. The degradation of the nanocrystals increases the number of deep-level defects; thus increases the wide band yellow emission. For sample II (see Fig. 3(b)), there is no such behavior. Both of the samples have the same PL peak positions. But the relative intensities of peaks 1–3 are different between samples I and II. Peak1 is ascribed to surface defects, considering the fact that peak1 changes with the annealing temperature [12]. Peak2 and peak3 in samples do not change with the annealing temperature, indicating that they correspond to deep-level defects. Some researchers [8,11,13] observed a broad emission spectrum ranging from 1.55 to 3.10 eV with a peak at 2.25 or 2.82 eV. This peak is usually attributed to oxygen impurities or nitrogen vacancies [8,11,13]. According to our experiment, this peak can be attributed to oxygen impurities. In order to investigate the defects involved, the temperature dependant PL spectra of sample A0 is measured.

Fig. 6 shows the dependence of PL spectra on temperature in the range of 161–271 K for sample A0 excited at 325 nm. The main features of the PL spectra are

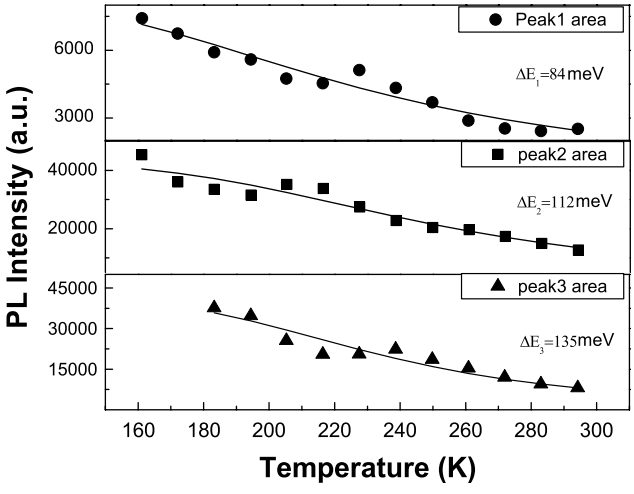

Fig. 7. The theoretical fit to the experiment data of AlN nanoparticles A0.

similar. By using a Gaussian line shape to fit the luminescence bands, three broad emission bands located at 2.07, 2.42, 2.98 eV, respectively, are obtained, as shown in Fig. 6. The locations of peaks remain unchanged with temperature, so the broad band is ascribed to deep-level defects. The linewidth is also insensitive to temperatures. The temperature dependence of the PL intensity can be expressed by the equation [14]

$$I(T) = \frac{I_0}{1 + A\exp(-\Delta E/k_B T)}$$

where ΔE is the activation energy of the thermal quenching process, k_B is Boltzman constant, I_0 is the emission intensity at 0 K, T is thermodynamic temperature, and A is a constant. The solid-line in Fig. 7 shows the theoretical fit to the experimental data. The following value of ΔE which are due to thermal ionization of defects are obtained: $\Delta E_1 =$ 84 meV, $\Delta E_2 = 112$ meV, and $\delta E_3 = 135$ meV, corresponding to 2.07, 2.42, 2.98 eV emission bands, respectively. Similar analysis can be performed for other samples. To our best knowledge, there is no report about the thermal ionization energy of the deep-level defects in literature.

4. Summary

AlN nanocrystals with diameter of approximately 4 nm were prepared in xylene at atmospheric pressure and low temperature. Two different phases AlN nanocrystals were obtained by changing the relative concentration of $AlCl_3$ and Li_3N in the Schlenk reaction system. The crystal structure of AlN nanocrystals in sample I was shown by XRD, to be a wurtzite structure. Cubic AlN nanocrystals with diameter of about 4 nm could be obtained when annealed at 600 °C with AlN powder of sample II. Photoluminescence spectra indicated that the broad band emissions could be ascribed to surface and deep-level defects with a yellow luminescence band centered at 2.42 eV in AlN.

Acknowledgements

This work was supported by the National Natural Science Foundation of China No. 60176003, 603176009 and 60278031.

References

[1] G. Long, L.M. Foster, J. Am. Ceram. Soc. 42 (1959) 355.
[2] W.D. Kingery, J. Francl, R.L. Coble, T. Vasilos, J. Am. Ceram. Soc. 37 (1954) 107.
[3] S.D. Mark Jr., R.C. Emanuelson, Am. Ceram. Soc. Bull. 37 (1958) 193.
[4] K.M. Taylor, C. Lenie, J. Electrochem. Soc. (1960) 308.
[5] L. Trinkler, P. Christiansen, N.A. Larsen, B. Berzina, Radiat. Meas. 29 (1998) 341.
[6] T. Barfels, H.J. Fitting, A. Gulans, J. Jansons, M. Springis, H. Stolz, I. Tale, A. Veispals, Radiat. Meas. 33 (2001) 709.
[7] Y.C. Lan, X.L. Chen, Y.G. Cao, Y.P. Xu, L.D. Xun, T. Xu, J.K. Liang, J. Cryst. Growth 207 (1999) 247.
[8] X.P. Hao, M.Y. Yu, D.L. Cui, X.G. Xu, Y.J. Bai, Q.L. Wang, M.H. Jiang, J. Cryst. Growth 242 (2002) 229.
[9] Y.G. Cao, X.L. Chen, Y.C. Lan, J.Y. Li, Y.P. Xu, T. Xu, Q.L. Liu, J.K. Liang, J. Cryst. Growth 213 (2000) 198.
[10] W.N. Smith, J. Organomet. Chem. 82 (1974) 1.
[11] G.A. Stack, T.F. McNelly, J. Cryst. Growth 34 (1976) 263.
[12] P. Jonnard, C. Bonnelle, G. Blaise, G. Rémond, C. Roques-Carmes, J. Appl. Phys. 88 (2000) 6413.
[13] W.M. Yim, et al., J. Appl. Phys. 44 (1973) 292.
[14] D.S. Jiang, H. Jung, K. Ploog, J. Appl. Phys. 64 (1988) 1371.